Analytica Chimica Acta 1172 (2021) 338681

Contents lists available at ScienceDirect

Analytica Chimica Acta

journal homepage: www.elsevier.com/locate/aca

Application of tetrahedral -deoxyribonucleic acid electrochemistry platform coupling aptazymes and hybridized hairpin reactions for the measurement of extracellular adenosine triphosphate in plants

Guoyan Zhao [a], Yongmei Liu [a], Jie Du [a, b, *], Huizi Zhang [a], Hanqing Feng [a, **], Xiaoquan Lu [b, ***]

[a] College of Life Science, Northwest Normal University, Lanzhou, 730070, Gansu, China
[b] Key Laboratory of Bioelectrochemistry & Environmental Analysis of Gansu Province, Northwest Normal University, Lanzhou, 730070, Gansu, China

HIGHLIGHTS

- Novel T-DNA-based electrochemical aptazyme sensor for detecting ATP was designed.
- Signal amplification was achieved by coupling aptazymes with HCR and SNAzymes.
- The method showed high selectivity and detected extracellular ATP in plants.

GRAPHICAL ABSTRACT

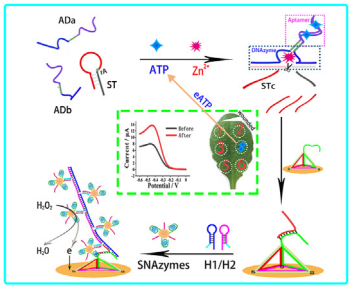

ARTICLE INFO

Article history:
Received 4 February 2021
Received in revised form
18 May 2021
Accepted 21 May 2021
Available online 24 May 2021

Keywords:
Extracellular adenosine triphosphate
Electrochemical biosensor
Tetrahedral deoxyribonucleic acid
Aptazyme
Hybridization chain reaction

ABSTRACT

Extracellular ATP (eATP) is an important biological signal transduction molecule. Although a variety of detection methods have been extensively used in ATP sensing and analysis, accurate detection of eATP remains difficult due to its extremely low concentration and spatiotemporal distribution. Here, an eATP measurement strategy based on tetrahedral DNA (T-DNA)-modified electrode sensing platform and hybridization chain reaction (HCR) combined with G-quadruplex/Hemin (G4/Hemin) DNAzyme dual signal amplification is proposed. In this strategy, ATP aptamer and RNA-cleaving DNAzyme were combined to form a split aptazyme. In the presence of ATP, this aptazyme hydrolyzes the cleaving substrate strand with high selectivity, releasing cleaved ssDNA, which are captured by the T-DNA assembled on the electrode surface, triggering an HCR on the electrode surface to form numerous linker sequences of the HCR dsDNA product. When G-quadruplex@AuNPs (G4) spherical nucleic acid enzymes (SNAzymes) with other linkers are used as nanocatalyst tags, they are captured by HCR dsDNA through sticky linkers present on the electrode surface. An amplified electrochemical redox current signal is generated through SNAzyme-mediated catalysis of H_2O_2, enabling easy detection of picomole amounts of ATP. Using this strategy, eATP levels released by tobacco suspension cells were accurately measured and the distribution and concentration of eATP released on the surface of an Arabidopsis leaf was determined.

* Corresponding author. College of Life Science, Northwest Normal University, Lanzhou, 730070, Gansu, China.
** Corresponding author.
*** Corresponding author.
E-mail addresses: dujie@nwnu.edu.cn (J. Du), fenghanq@nwnu.edu.cn (H. Feng), luxq@nwnu.edu.cn (X. Lu).

https://doi.org/10.1016/j.aca.2021.338681
0003-2670/

1. Introduction

Adenosine triphosphate (ATP), as one of the indispensable energy-carrying molecules and genetic building blocks of living organisms, plays an important role in a variety of physiological and pathophysiological processes. In plants, ATP is released from cells and into the extracellular matrix in response to a variety of environmental stresses, including biotic and abiotic stresses [1–3]. Recent evidence suggests that extracellular ATP (eATP) in plants can stimulate intracellular calcium responses, and the eATP signaling pathway interacts with other signaling pathways of classical defense hormones (i.e., jasmonate, ethylene, and salicylate) and acts as a damage-associated molecular pattern molecule [4–7]. eATP is now recognized as an important extracellular signaling molecule in plants [8,9]. However, the lack of availability of efficient and direct methods for quantitative analysis of eATP dynamics in plant organs and tissues implies that the mechanism mediating signaling remains poorly understood. The traditional detection technologies for ATP are high-performance liquid chromatography [10,11], mass spectrometry [12,13], and the luciferin-luciferase assay [14,15]. Although widely used, usage of expensive equipment, complex handling procedures, frequent pretreatment, and operation by skilled personnel are notable aspects that are time-consuming, limit applicability, and pose challenges in the monitoring of low concentrations of ATP in the complex extracellular matrix. Therefore, the development of novel approaches capable of being utilized for rapid and precise quantification of eATP changes inside plant tissues is warranted.

The aptamer-based strategy has been popularly employed in pattern biosensing platforms for biomolecules, due to the aptamer's high affinity for targets, convenient synthesis, design flexibility and good stability. A variety of aptamer-based sensors, utilized using fluorescence [16,17], colorimetry [18,19], and electrochemistry [20,21] for signal readouts, have been established for sensitive and selective detection of ATP. Few sensors them even can offer superb high specificity to necessary for monitoring of intracellular ATP levels [22]. Despite its advantage of exhibiting a simple and universal design, however, measurable signals typically is directly mirrored from conformational changes in the aptamer and are typically associated with the bind to the target. The determination of such signals is challenging for precise quantification, especially for eATP in extracellular environment which is in present at extremely low concentrations in the extracellular environment. To improve sensitivity, various nucleic acid amplification techniques including strand displacement amplification (SDA) [23], exonuclease-assisted recycling amplification [24], rolling circle amplification (RCA) [25], hybridization chain reaction (HCR) [26], catalytic hairpin assembly (CHA) [27], and utilization of DNAzymes [28] have been incorporated in aptamer-based sensing strategies.

Recently, the fusion of aptamers with RNA-cleaving DNAzymes, termed for the development of aptazymes [29] has drawn increasing attention. Aptazymes are designed to possess the recognition capability of aptamers and the catalytic cleaving activity of DNAzymes, where binding of the aptamers subunit to the target molecule results in significant conformational changes, thereby triggering the catalytic activity of the DNAzyme subunit [30,31]. Activated aptazymes can then catalyze the cleavage of nucleic acid substrate sequences, resulting in the release of shorter nucleic acid sequences. Interestingly, few studies have used cleavage events of DNAzymes or aptazymes to release shorter sequences, which as initiator sequences, can trigger other nucleic acid amplification circuits such as HCR or CHA. Recently, few aptazyme-based methods that result in the cascade of multi-amplification processes have been exploited in the detection of a variety of low abundance biomolecules [32]. For example, Li et al. recently proposed an electrochemical biosensing platform for detection of ATP based on coupling aptazymes and CHA, in which the shorter sequence released from aptazyme substances could open a hairpin DNA anchored directly on the surface of the electrode, further triggering an in situ CHA process, leading to a high turnover signal amplification [33]. Similar studies where HCR, RCA, and SDA were combined with electromechanical devices have also been demonstrated [34–36]. Owing to the advantages of the electrochemical technique, these coupled cascade strategies had quick response, low cost, facile operation, and portability, and remarkably improved sensing capability. However, controlling the nucleic acid amplification process and positioning the high-order capture probe onto the surface of conductive supports to construct the sensing platform poses challenges. The performance of the biosensor is usually negatively affected by the density and orientation of DNA at the heterogeneous electrode interface.

Tetrahedral DNA (T-DNA) nanostructures are a type of three-dimensional nucleic acid framework assembled from four single-stranded DNAs (ssDNA). Owing to their simple design, high-order structure, and remarkable stiffness, they have been actively explored in the design of biosensor interfaces [37–39]. A study conducted by Fan et al. reported the development of various electrochemical biosensing platforms based on T-DNA nanostructures for the sensitive detection of nucleic acids, proteins, small molecules, and cells [40–42]. Wang et al. developed an exosome-based electrochemical aptasensor which combined T-DNA nanostructures with exosome aptamers to form a sensing interface [43]. An electrochemiluminescence (ECL) biosensor combining HCR amplification with tetrahedral DNA nanostructures was established by Zhu et al. In this biosensor, T-DNA nanostructures were grafted onto the electrode surface to form the connector, to reduce the hindrance effect of probes, and to improve the hybridization efficiency of nucleic acid molecules, resulting in the ultrasensitive detection of miRNA-133a with a detection limit of 12.17 aM [44]. Furthermore, Bu et al. adopted the tetrahedron structure to develop an ECL aptasensor intended to be used for ATP detection [45]. These studies show that T-DNA can provide a nanoengineered interface for spatial control with excellent structural stability, specific orientation, and well-defined spacing on solid surfaces, indicating that there is considerable potential in the exploration of a DNA nanostructure-based electrochemical platform.

In this study, we proposed a sensing strategy based on the T-DNA electrochemistry platform coupling aptazymes and HCR for the ultrasensitive and selective detection of targets. As described in Scheme 1, ATP-specific aptazymes consisting of two separate fragments were designed. These were used to specifically recognize ATP and to convert signals from ATP to shorter ssDNA strands. The T-DNA modified electrodes on which shorter ssDNA strands were captured were then constructed, triggering HCR on the surface of the electrode, and leading to the amplification of the converted signal. Finally, spherical nucleic acid DNAzymes (SNAzymes), that are constructed by assembling thiolated G-quadruplex (G4) and linker strands on AuNP surfaces, were used as nanozyme electrochemical signal tags, which are anchored by linker sequences to the HCR dsDNA to obtain an amplified current response. Considering the features of this design, the proposed strategy is highly selective, and multiple amplifications can be achieved at detection limits as low as 5 pM. Additionally, this detection approach requires an extremely small ATP sample volume. Using an in-situ sample preparation protocol, this strategy was used to measure eATP levels released from an Arabidopsis leaf and to map its spatial distribution. This study demonstrated that this design afforded a promising strategy for the measurement of extracellular ATP levels, and because diverse aptamers could be obtained through *in vitro* selection, this platform might be further used for the precise

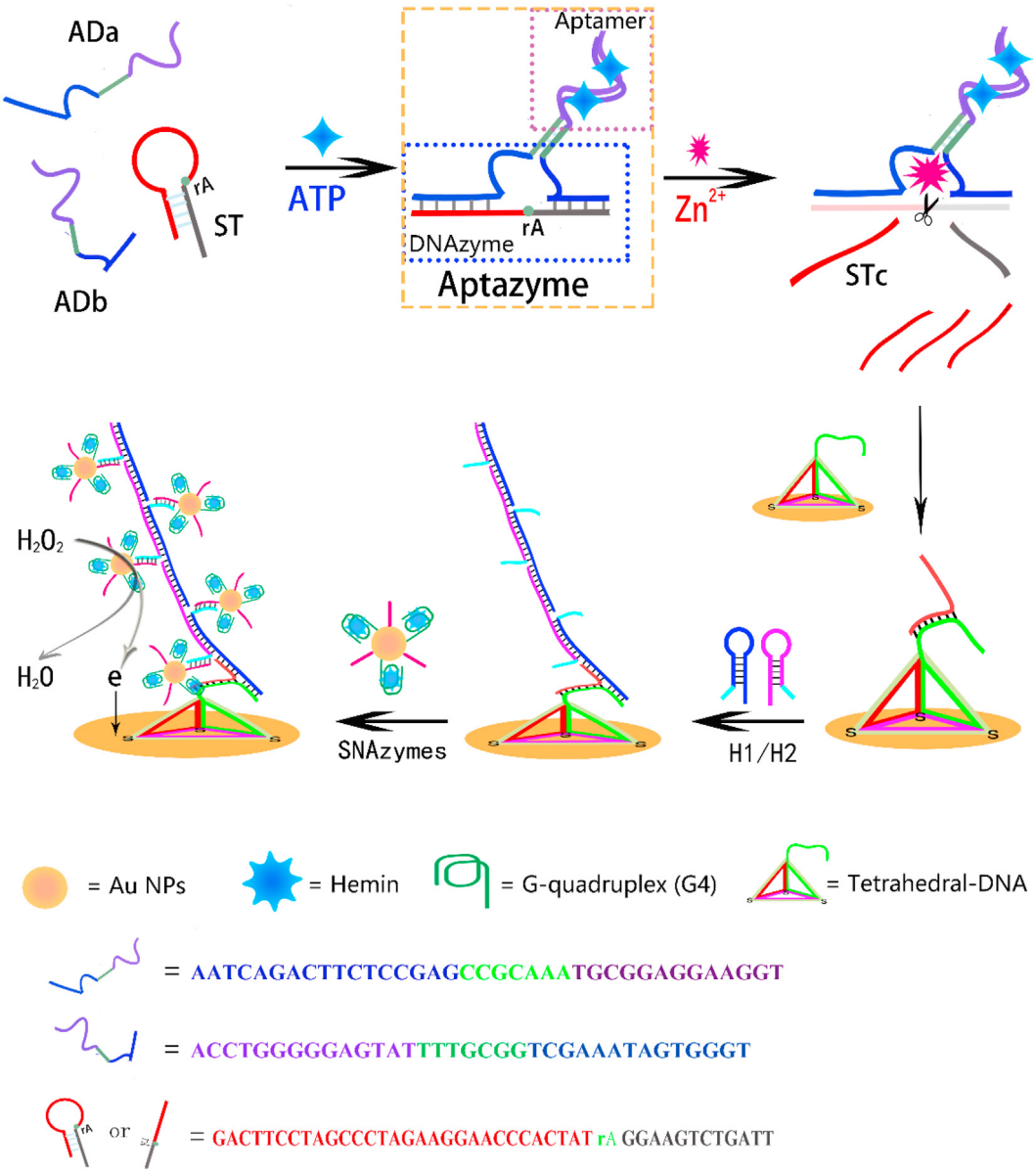

Scheme 1. Schematic illustration of electrochemical detection of ATP based on the target-induced formation of aptazymes as a converter to trigger HCR coupling with SNAzyme to achieve signal amplification.

detection of various targets encountered in bioanalytical and clinical settings.

2. Materials and methods

2.1. Reagents and instrumentation

All DNA oligonucleotides used in this work were synthesized and purified by Sangon Biotech Co., Ltd. (Shanghai, China), and the sequences are listed in Table S1 (See the Supporting Information). All used nucleic acids in this study were denatured at 90 °C for 10 min before use. Adenosine triphosphate (ATP), cytidine triphosphate (CTP), uridine triphosphate (UTP), guanosine triphosphate (GTP), Tris(2-carboxyethyl) phosphine hydrochloride (TCEP),6-mercapto-1-hexanol (MCH) and Firefly Lantern Extract were bought from Sigma-Aldrich Co., Ltd. (Shanghai, China). Hemin and chloroauric acid ($HAuCl_4$) were purchased from Aladdin Reagents (Shanghai, China). All other reagents were of analytical grade and directly used without further purification. Ultrapure water with a resistivity of 18 MΩ cm was used in whole experiments.

The cleavage buffer of ATP-induced aptazymes is the mixture of 10 mM Tris-HCl buffer (pH 7.4), 100 mM NaCl, 10 mM $MgCl_2$ and 250 μM $ZnCl_2$. HCR buffer contains 10 mM Tris-HCl (pH 7.4), 100 mM NaCl and 10 mM $MgCl_2$. The TM buffer for the synthesis of T-DNA contains 17.2 mM Tris base, 43 mM of $MgCl_2$ (pH 8.0). Phosphate buffered solutions (PBS, pH 7.0) containing 20 mM Na_2HPO_4, 20 mM NaH_2PO_4 and 0.1 M KCl were used throughout the experiment.

Cyclic voltammetry (CV), line scan voltammetry (LSV) and electrochemical impedance spectroscopy (EIS) were measured using a CHI 760e electrochemistry workstation (Shanghai Chenhua

Apparatus Inc., China). A three-electrode system including an Au working electrode (diameter 3 mm), an Ag/AgCl reference electrode, and a platinum wire counter electrode was adopted for the electrochemical workstation. The CV and EIS measurements were conducted in 5 mM $[Fe(CN)_6]^{3-/4-}$solution containing 0.1 M KCl, EIS with the frequency range of 0.1–10 kHz and amplitude of 5 mV. The gel electrophoresis images were taken by a GelDoc gel imaging system (Bio-Rad Laboratories, Inc.). Atomic force microscope (AFM) image was obtained by Nanoscope IIIa-Multimode (Veeco-Digital Instruments). UV–visible spectroscopy was obtained on a UV-1800 spectrophotometer (Shimadzu).

2.2. Synthesis and characterization of T-DNA and SNAzymes

T-DNA composed of four specifically designed ssDNA (S1, S2, S3, and S4; Table 1), was added to the TM buffer to achieve a final concentration of 1 μM. The mixture was preheated to 95 °C (approximately 5 min) to fully denature the ssDNA and then rapidly cooled to 4 °C for 1 min, as per methods reported previously [43]. Polyacrylamide gel electrophoresis (PAGE) was performed to characterize ssDNA and T-DNA. T-DNA morphology was documented using atomic force microscopy (AFM). The final T-DNA solution (1 μM) was stored at 4 °C until further use.

To generate SNAzymes, AuNPs were first synthesized by boiling aqueous $HAuCl_4$ (0.1 mM) and sodium citrate. Thereafter, AuNPs were incubated with a mixture of thiolated linker DNA (500 nM) and G4 DNA (1 μM) overnight at 25 °C to enable the formation of spherical nucleic acids (SNAs). The SNAs were then subjected to washing as salt deposits and UV–visible spectroscopy was performed to record the monitored loading of DNA (Fig. S1), as per protocols reported previously [46,47]. SNAs were allowed to undergo folding in the presence of K^+ and then complexed with hemin to form SNAzymes. Final SNAzymes was ultra-filtered using PBS to remove excess hemin and stored at 4 °C until further use.

2.3. Preparation of the T-DNA electrode

The Au electrode (AuE) was polished, first using 0.3 μm and then using 0.05 μm of alumina powder, to obtain a mirror surface. This was followed by subjecting the electrode to three ultrasonic washes using ethanol and water, and then drying at room temperature. Subsequently, 5 μL of 1 μM tetrahedron DNA in an immobilization buffer (containing 5 mM TCEP, freshly prepared) was dropped onto the surface of the cleaned gold electrode and a centrifuge tube was used to cap the electrode to prevent evaporation. After 1 h incubation at room temperature, the T-DNA-modified electrodes were exposed to 2 mM MCH solution at room temperature for 30 min to eliminate nonspecific binding [48].

2.4. ATP detection

To detect ATP, aptazyme activation and DNA substrate cleavage were first conducted. For this, 18 μL of the cleavage buffer containing aptazymes (1 μM ADa, 1 μM ADb) and substrate strands (1.5 μM TS) was mixed with 2 μL of different concentrations of ATP solution and incubated for 120 min at 37 °C to initiate the enzymatic cleavage reaction. Then, 10 μL of the cleavage product was transferred onto the T-DNA electrode and incubated for 30 min at 37 °C to allow the capture of shorter DNA strands. The electrodes were subsequently rinsed thoroughly using Tris-HCl buffer, the resulting electrode was immersed into HCR buffer containing H1 (2 μM) and H2 (2 μM), and incubated 37 °C for 60 min. Finally, 5 μL of SNAzymes was dropped onto the electrode; the electrode was incubated at 37 °C for 30 min and then subjected to washing. Linear sweep voltammetry (LSV) was performed for the resulting electrode using PBS (20 mM, pH 7.4) containing 1 mM H_2O_2 at 0 to −0.6 V. (***Note**: Considering the complex nucleic acid structures may be unstable after long-term storage, so LSV should be performed immediately after electrode construction finished. See Fig. S5*).

2.5. Collection and preparation of eATP samples

To obtain eATP from the suspension cell medium, transfer 500 μL of subculturing tobacco cells to cell culture plate containing 3 mL of MSMO medium without ATP and incubate in dark at 23 °C, 150 rpm. After 5 days subculturing, a cell strainer is inserted into the wells, and the culture medium containing eATP is gently collected. The samples were boiled at 96 °C for 5 min to denature ATP-degrading enzymes, cooled at 4 °C and then stored at −20 °C prior to conducting ATP measurements. ATP levels were assayed using the Firefly Lantern Extract, with luciferase catalyzing the release of photons following the reaction between ATP and luciferin, according to the manufacturer's instructions [49].

To measure eATP levels released from Arabidopsis leaves, Arabidopsis seeds were planted in standard MS media and allowed to grow for two weeks under constant light conditions at 22–25 °C. Wounds on one leaf from the two-week-old seedling were inflicted by punching 2-mm holes through it; thereafter, 10 μL ATP-free deionized water was used as an extraction solution and dropped onto the surface of the leaf at a designated position (See Fig. 5). After 10 min, 2 μL of the extraction solution was collected to measure the levels of released ATP. Extraction solution collected from the leaf before inflicting wounds was used as a control [50]. ATP levels in these samples were measured using the procedures described above.

3. Results and discussion

3.1. Principles underlying the design strategy

The principle underlying the proposed approach for analyte detection is illustrated in Scheme 1. To achieve highly specific ATP recognition and effective signal conversion, the aptazymes, which were split into two segments (ADa and ADb), were first designed and chosen for subsequent analysis (See Supporting Information, Fig. S2). When the target ATP is present, it binds to the aptamer sequence, which contains two fragments (purple sequences indicating ADa and ADb, Scheme 1), respectively, inducing a split in the DNAzyme sequence (blue sequences in ADa and ADb), thereby causing it to fold and hybridize with the substrate DNA (ST) for the

Table 1
Recovery tests for ATP in diluted suspension cell medium samples.

Sample	Content of ATP/pM	Added/pM	Found/pM[b]	Recovery/%	RSD/%
Tobacco extracellular ATP	107.00[a]	50	160.32	106.34	2.55
		100	209.12	101.97	3.47
		200	302.33	97.59	2.36

[a] This concentration was derived from the measurement of ATP using the ATP luciferase KIT.
[b] The average value of six measurements.

formation of the active aptazyme. Then, under the action of zinc ions, the adenosine ribonucletide (rA) site of the substrate DNA is hydrolyzed and cleaved, and the shorter ssDNA (denoted as STc, indicated by the red sequence) is released, leading to conversion from ATP to shorter ssDNA fragments. T-DNA, which is self-assembled on the surface of the electrode through the thiol groups of three vertexes, is used to capture shorter ssDNA fragments as the signal amplification scaffold. In the T-DNA, another vertex contains an open sequence (capture strand, denoted as CS, indicated by the green sequence), that has a partially complementary sequence with shorter ssDNA fragments. In the absence of shorter ssDNA fragments, the formation of a rigid duplex between the capture strands and the shorter ssDNA fragments not only completes the transfer of DNA from the solution to the surface of the electrode, but also facilitates the formation of a Y-type DNA substructure and triggers HCR oligomerization. In the Y-type substructure, a linear ssDNA region of 24 nucleotides, which contains a part of the 5′ end of CS and a part of the 3' end of STc, was designed. It could exhibit hybridization with H1 and enable opening of the hairpin structure, subsequently triggering HCR to produce a long DNA concatemer with multiple linkers. Spherical nucleic acid nanoprobes (SNAzymes), constructed by assembling thiolated G-quadruplex (G4) and linker strands on AuNP surfaces [46,47], were used as signal amplification probes. Each fuel strand end of the HCR (H1 and H2) contains a complementary linker, allowing localization of numerous SNA probes on the electrode and estimation of the amount of SNAzymes related to HCR oligomerization. G4 binding with hemin undergoes assembly to form peroxidase-mimics (G4/hemin DNAzyme) which catalyze the deoxidation of H_2O_2; thus, a significant increase in electrochemical signal can be available for the occurrence of signal amplification. Finally, the concentration of ATP could be calculated by detecting the electrochemical current signals arising from H_2O_2.

3.2. Feasibility of the designed strategy

Aptazymes used in this work were based on Zn^{2+}-dependent DNAzymes [51] and and a well-characterized ATP aptamer [52], which were cut and fused to form split-type aptazymes (ADa and ADb). To validate the selectivity and signal conversion capability of the aptazymes, substrate strand cleavage was assessed using denatured polyacrylamide gel electrophoresis (dPAGE) analysis. Fig. 1A shows the denatured gel; lanes 1 and 2 contained the aptazyme and substrate strand, respectively; lane 5 contained a mixture of the two, but without ATP; lanes 6–8 contained a mixture of these, but with ATP. As expected, after incubation for 3 h, a new, relatively low-molecular-weight band was observed in the ATP-included systems (lanes 6–8). Moreover, the brightness of the new band increased with increased ATP concentration, suggesting that this band corresponded to the cleavage products of the substrate strand. The aptazyme system could not cleave the substrate strand in the absence of ATP (lane 5). This was also true for the control experiments conducted using contents in lanes 3 and 4 where cleavage did not occur. These results demonstrated that the catalytic activity of these aptazymes could be induced via ATP-aptazyme binding, leading to the cleavage of the substrate strand [33], which would then allow the occurrence of analyte-recognition events resulting in the release of shorter DNA fragments.

Next, the STc, which when combined with the As-strand acts as an initiator of HCR, was examined, and PAGE was performed to verify the success of the HCR performed. As shown in Fig. 1B, the clear bands from lanes 1 to 4 correspond to H1, H2, H1+H2, and H1+H2+CS, respectively. When STc was incubated with the CS and H1 + H2 mixture, a series of stripes with higher molecular weights were observed (lane 5), indicating that a cascade of hybridization events was triggered. Thereafter, STc was replaced with the cleavage product of aptazymes to trigger HCR, and an evident band of the HCR product was observed in lane 6. Additionally, the secondary structures of these sequences and the underlying hybridization reaction were theoretically simulated using the NUPACK software (http://www.nupack.org/). These simulated results conclusively confirmed the design of the DNA sequences, which could be successfully used to conduct HCR and to enable the formation of a long dsDNA concatemer containing a Y-type DNA substructure (Supporting Information, Fig. S3).

Fig. 1C shows the electropherogram of the T-DNA assembly process. Lanes 1–4 correspond to S1, S1+S2, S1+S2+S3, and S1+S2+S3+S4, respectively. As expected, the migration rate of the hybrid products of the four ssDNA (lane 4) fragments was markedly slower than that of any single DNA strand and the other combinations of two or three sequences. Atomic force microscopy (AFM) was then performed to elucidate the morphology of T-DNAs [45]. As shown in Fig. 1D, the AFM image exhibits the existence of a well-dispersed nanostructure. These results suggested that the DNA tetrahedron nanostructure was successfully assembled and could result in a high yield.

Electrochemical impedance spectroscopy (EIS) was used to characterize the different modification stages of the electrode surface, since the semicircular diameter denotes the strength of charge transfer resistance (R_{ct}) at the electrode interface. As shown in Fig. 2A, the bare Au electrode (AuE) is indicated by the smallest semicircle (curve a). The semicircle domain then increases with the sequential immobilization of T-DNA (curve b), MCH (curve c), and STc (curve d), which can be ascribed to the barrier function of the negatively charged DNA in the $[Fe(CN)_6]^{3-/4-}$ electron transfer [46]. After the introduction of H1 and H2 to trigger an HCR, there was a difficulty in performing electron transfer due to the surface confinement of the dsDNA concatemer, resulting in exhibition of a further enlarged semicircle domain (curve e). Finally, when capturing the labeled SNAzymes (Fig. 2A, curve f), the semicircle domain showed further enlarged compared with curve e, and this was attributed to the G4 structure and hemin on the surface of SNAzyme would interfere with electron transfer, which making the SNAzyme/HCR/STc/MCH/T-DNAs/AuE have more the resistance of charge transfer (Rct). Furthermore, cyclic voltammetry was also used to provide further information on the preparation of the modified electrodes (Supporting Information). As shown in Fig. S4, the characteristic redox peaks of $[Fe(CN)_6]^{3-/4-}$ were first observed during the analysis of the bare Au electrode (curve a). When T-DNAs, MCH, STc, and concatemers of HCR are gradually added to the electrodes, the redox peak current decreases in a stepwise manner (curve b–e). With the final introduction of SNAzymes, the redox peak current also is decreased (curve f), indicating that the SNAzymes had been captured, which was consistent with EIS results. These experimental results clearly demonstrate the feasibility of this sensing platform.

To validate the signal amplification performance of the G4/hemin DNAzyme, their peroxidase-like ability to catalyze the oxidation of TMB was tested. As shown in Fig. 2B, two pairs of characteristic peaks (at 0.23 and 0.38 V) were observed (curve a), which were the oxidation peak currents of the electrode for TMB [53]. When a complete, modified electrode with SNAzymes was CV in solution TMB (curve c), an evidently increased reduction current response was observed compared with the response in the absence of hemin (curve b). The oxidation peak current of the SNAzyme/HCR/STc/MCH/T-DNAs/AuE for TMB was significantly increased compared with that of T-DNAs/AuE, these results indicating the existence of a typical peroxidase-mimicking electrocatalytic process on SNAzyme/HCR/STc/MCH/T-DNAs/AuE [53,54]. LSV measurements were used to further verify the feasibility of the

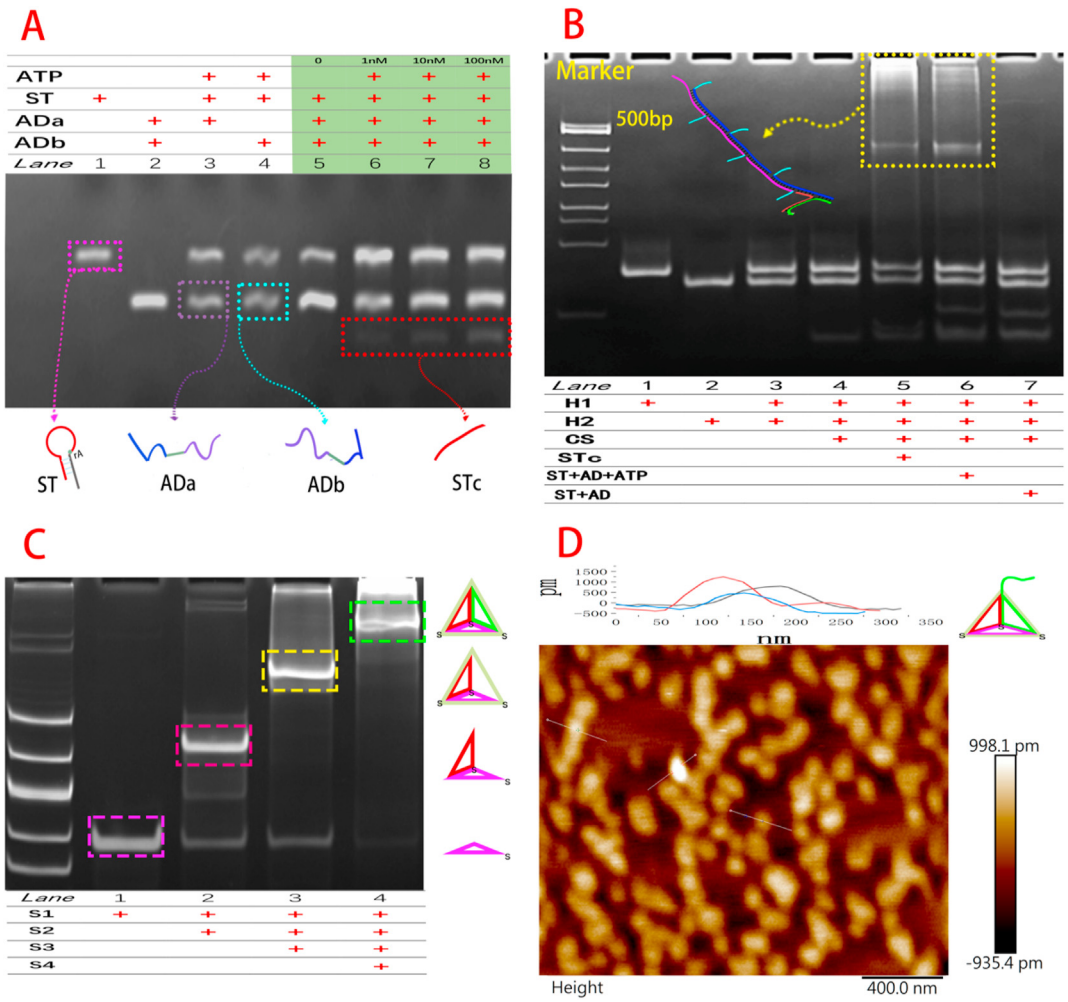

Fig. 1. (A) Denatured gel electrophoresis-based characterization of the catalyzed cleavage of the aptazyme system; (B) native gel electrophoresis-based characterization of the triggered HCR; (C) native gel electrophoresis-based characterization of the assembled T-DNA; (D) AFM image and cross-sectional analysis of the T-DNA. The '+' sign denotes the presence of the corresponding components.

designed amplification process in PBS containing 1 mM H_2O_2. As shown in Fig. 2C, a well-defined LSV peak at approximately −0.39 V was observed in the presence of target ATP and SNAzymes (curve c). In contrast, no peak current was observed at the T-DNA electrode (curve a). Thus, this peak may be attributed to the electrochemical reduction of H_2O_2 by the hemin/G-quadruplex [55–57]. To For further confirmation, the i-t of HCR/STc/MCH/T-DNAs/AuE and SNAzyme/HCR/STc/MCH/T-DNAs/AuE (from 1 nM ATP) at initial E = −0.39V were recorded upon continuous addition of 0.1 mM H_2O_2. Fig. S6 shows that current response increased with the increase of H_2O_2 concentration, the current change of modified electrode with SNAzymes is more significant than that of modified electrode without SNAzyme, these results also confirm that the SNAzymes is highly electrocatalysis activity to H_2O_2. These results suggesting that these SNAzymes can be utilized as nanocatalyst signal tags for ATP detection.

3.3. Optimization of experimental conditions

To achieve the best analytical performance, several experimental parameters were optimized. The effect of the assembled T-DNA was first examined based on the electrochemical response to target ATP detection. As illustrated in Fig. 3A, the LSV peak current response was measured over a 30–240 min incubation period, and an incubation period of 60 min showed the best LSV peak current response triggered. Although longer periods of incubation can increase the assembly density on the electrode surface, high density T-DNA may restrict the capturing efficiency of SNAzymes to the dsDNA concatemer owing to the presence of the steric hindrance effect [58]. Thus, 60 min was selected as the optimal assembly time for T-DNA in subsequent detection experiments. Changes in the LSV peak current responses with increasing HCR time are shown in Fig. 3B. When HCR time was longer than 120 min, the LSV peak current did not visibly change; therefore, 120 min was considered for conducting HCR. Other parameters, including the concentrations of hemin and H_2O_2, were also optimized. Fig. 3C and D show that the best LSV response was obtained at 20 μM hemin and 1 mM H_2O_2, respectively. Besides, LSV parameters also were optimized, the potential window is chosen at 0 to −0.6 V and scan rate is 50 mV (Details please see Supplementary material).

3.4. Sensitivity and selectivity of the sensing platform

Based on the optimized experimental conditions selected above, the sensing platform for ATP detection was examined using various concentrations of target ATP. As shown in Fig. 4A, the LSV peak current increased when the concentration of target ATP increased from 0 to 10 nM, indicating that the capture of the SNAzymes on the

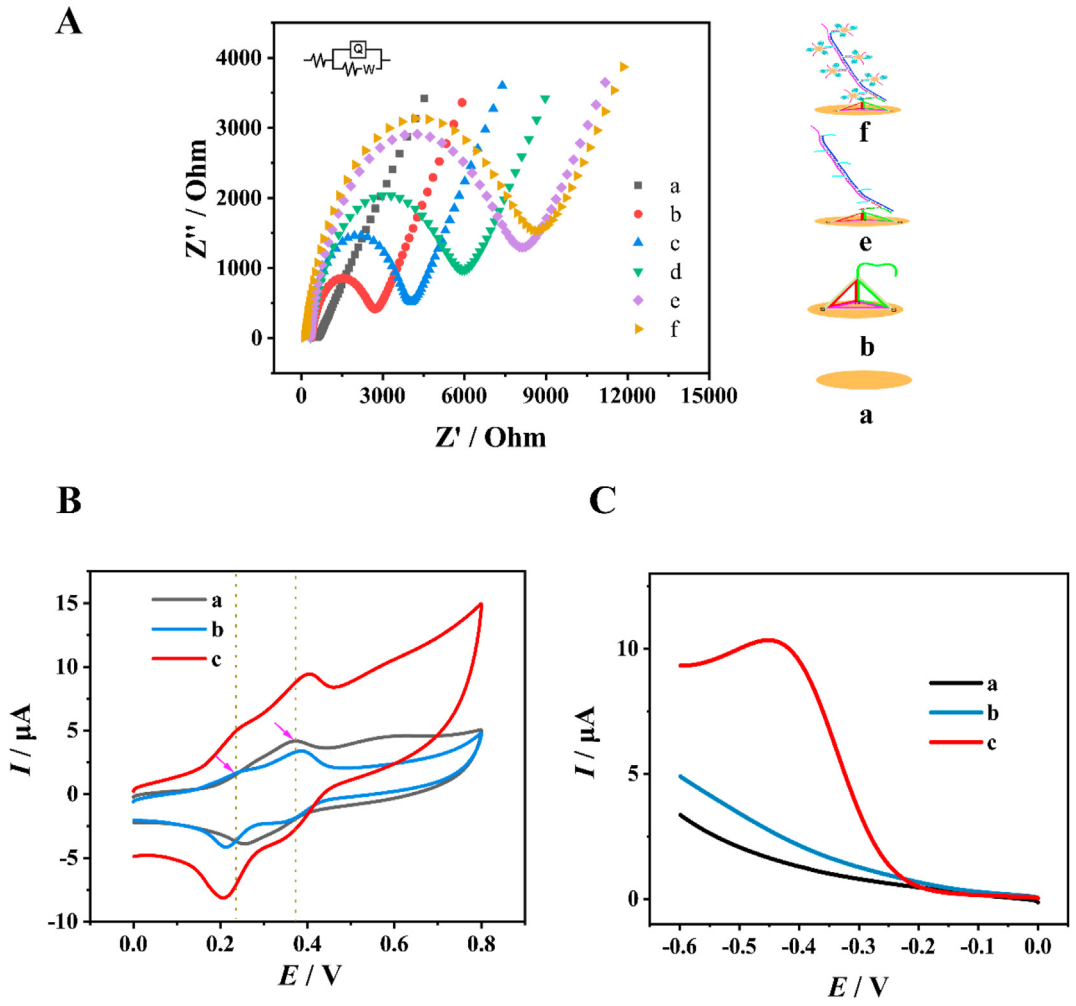

Fig. 2. (A) EIS characteristics of different electrodes in 0.1 M KCl aqueous solution containing 5 mM $[Fe(CN)_6]^{3-/4-}$ as redox probe: (a) Bare AuE, (b) T-DNAs/AuE (c) MCH/T-DNAs/AuE, (d) STc/MCH/T-DNAs/AuE, (e) HCR/STc/MCH/T-DNAs/AuE, and (f) SNAzyme/HCR/STc/MCH/T-DNAs/AuE. EIS was performed at 0.1 Hz–100 kHz frequency range; (B) CV characteristics of the different electrodes in 20 mM PBS buffer containing 0.1 mM TMB: (a) T-DNAs/AuE, (b) HCR/STc/MCH/T-DNAs/AuE, (c) SNAzyme/HCR/STc/MCH/T-DNAs/AuE; (C) LSV responses of the different electrodes in 20 mM PBS buffer containing 1 mM H_2O_2 with scan rate of 50 mV s-1: (a) T-DNAs/AuE, (b) HCR/STc/MCH/T-DNAs/AuE, (c) SNAzyme/HCR/STc/MCH/T-DNAs/AuE. The HCR/STc/MCH/T-DNAs/AuE and SNAzyme/HCR/STc/MCH/T-DNAs/AuE were determined at a concentration of 1 nM ATP.

electrode was highly dependent on the concentration of target ATP. This confirms the working principle that target ATP induces the release of shorter DNA strands which trigger HCR. As illustrated in Fig. 4B, the LSV peak current was proportional to the concentration of the target ATP in the 0.01–10 nM range. The calibration curve showed a good linear correlation between the LSV current and logarithm of ATP concentration, and the regression equation $\Delta I = 4.94lgC(pM) - 4.50$ provided a correlation coefficient of 0.9982. The detection limit was estimated to be 5 pM (S/N = 3). Additionally, the established strategy included a satisfactory linear range and a relatively low LOD compared with other detection methods (Table S2 in Supplementary material). The results demonstrated that this signal amplification strategy was efficient for ultrasensitive electrochemical detection of ATP.

Apart from the determination of the detection sensitivity, it is also important to evaluate the selectivity performance of the ATP sensing platform. The selectivity of the strategy was investigated by assaying other ATP analogs such as CTP, GTP, and UTP. As shown in Fig. 4C, the LSV peak current showed no evident change when detecting 50 nM CTP, 50 nM GTP, and 50 nM UTP separately; however, a sharp increase in the LSV signal was observed in the presence of ATP at 5 nM. Furthermore, a mixture containing 50 nM GTP, 50 nM CTP, 50 nM UTP, and 5 nM ATP did not exhibit a remarkable difference in the LSV signal compared with that obtained using 5 nM ATP. These results demonstrated that this method had high selectivity against other nonspecific analogs.

To validate reliability of the developed method, the measurement results of this method in the spiked samples with the ATP concentration ranging from 10^{-10} M to 10^{-8} M were compared with results of luciferin-luciferase assay as the standard method (Table S3). The paired-sample *t*-test was performed, statistics results show $Prob = 0.23024$, $t = 1.4140$, $t_{(0.05)} = 2.776$, *and* $t < t_{(0.05)}$; *suggested* that there is no significant difference between the two groups of data at significance level 0.05. From these results, it can be concluded that the two methods are consistent with each other. Meanwhile, the robustness of the developed method also was examined using the five different modified electrodes (SNAzyme/HCR/STc/MCH/T-DNAs/AuE) obtained from 1 nM ATP by the same fabrication process. The results were represented in Fig. S7. It can see that The RSD of 5 modified electrodes were calculated as 1.198%. These results demonstrated that the developed mothed exhibited acceptable stability and reproducibility.

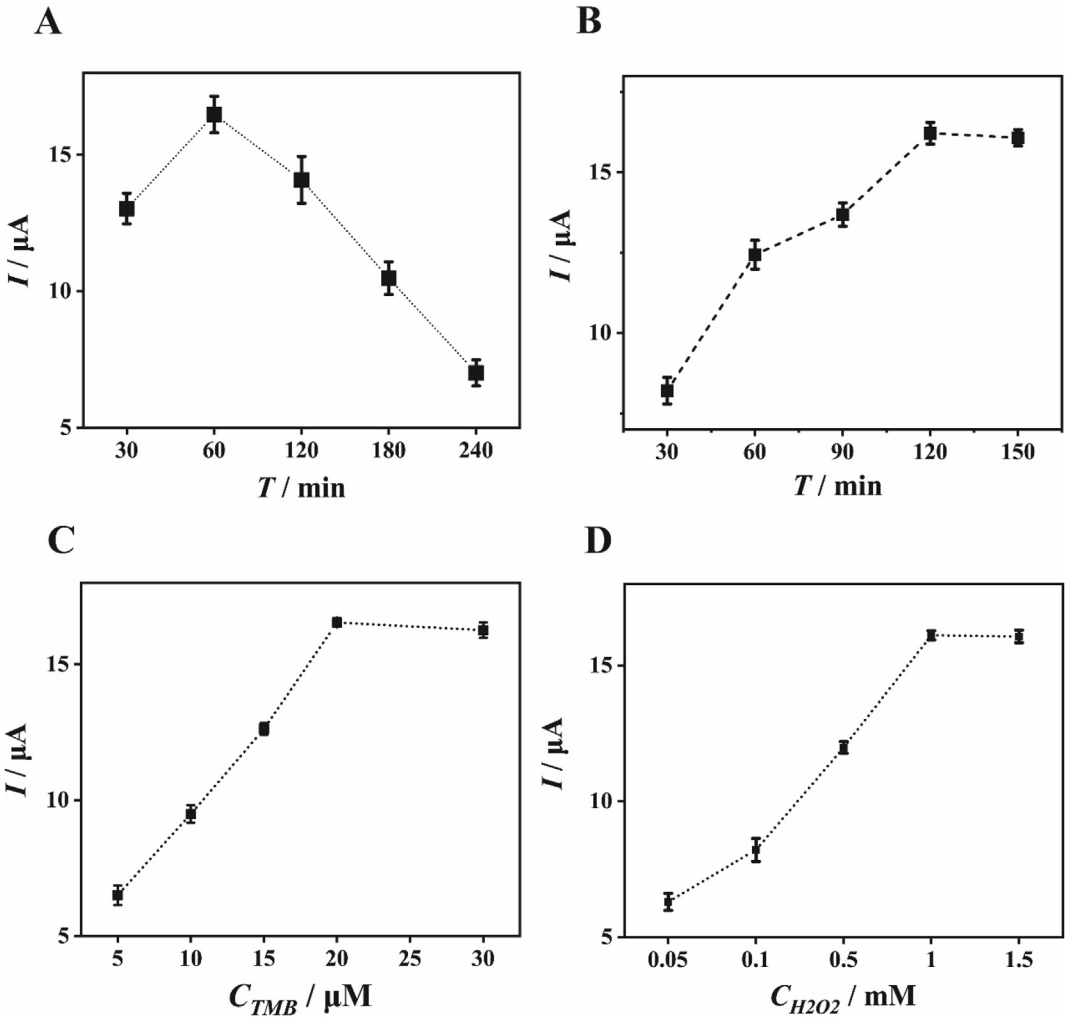

Fig. 3. Effects of (A) T-DNA assembly time; (B) HCR reaction time; (C) the TMB concentration; (D) the H_2O_2 concentration necessary for the detection of 10 nM ATP. The error bars indicate the standard deviation of three analyses.

3.5. Measurement of extracellular ATP in plants samples

To assess the practical application of the established strategy in biological samples, recovery experiments using the standard addition method were conducted. The concentrations of extracellular ATP in tobacco cell suspension culture media were first measured using the luciferase-luciferin reaction assay (10.7 nM); subsequently, different concentrations of ATP (50, 100, and 200 pM) were separately spiked into 100-fold diluted suspension media, and the samples were analyzed using the established strategy. The results are shown in Table 1. The recovery of the added ATP ranged from 97.59% to 106.34%, with RSD ranging between 2.36% and 3.47%, which proved that the proposed strategy could be successfully applied to monitor extracellular ATP levels in biological samples.

Few studies have shown that abiotic stresses, such as those caused by infliction of wounds, cause a marked increase in the eATP levels in plants [9,59]. For practical detection, one Arabidopsis leaf was locally wounded by inflicting an open cut, and the levels of eATP released on the surface of the leaf were monitored using the proposed method (for sample preparation, see experiment section). Fig. 5 shows the distribution of eATP levels at different sites of the leaf before and after infliction of the wounds. The concentration of eATP showed evident positional effect range (1.457−0.124 nM), as well as the mapping image of the ATP concentration of leaves provide more intuitive description (Fig. S8), which showed that eATP levels were elevated near the wounded sites. These results support the hypothesis that eATP is a universal signaling messenger released in response to highly dynamic stimuli [4,7,60], and suggests that the electrochemistry platform developed herein can help to evaluate the signaling role of eATP in plants in response to various stresses.

4. Conclusions

This study was performed to successfully develop a method involving aptazyme coupled with HCR electrochemistry for the ultrasensitive detection of ATP. The designed aptazymes could be used to recognize the induced allosteric sites, thereby enabling the formation of a highly selectivity assembly of DNAzymes for catalyzing the release of a considerable amount of shorter DNA fragments for signal transduction. Controlled T-DNA assembly on the surface of the electrode not only provides a good scaffold for HCR to allow signal amplification, but also enables the anchoring of nanocatalyst tags for signal output. Based on the strong catalytic ability of SNAzymes, amplification of the electrochemical signal was used to detect ATP in PBS containing H_2O_2, without the necessity of any additional probe activity. High accuracy and the

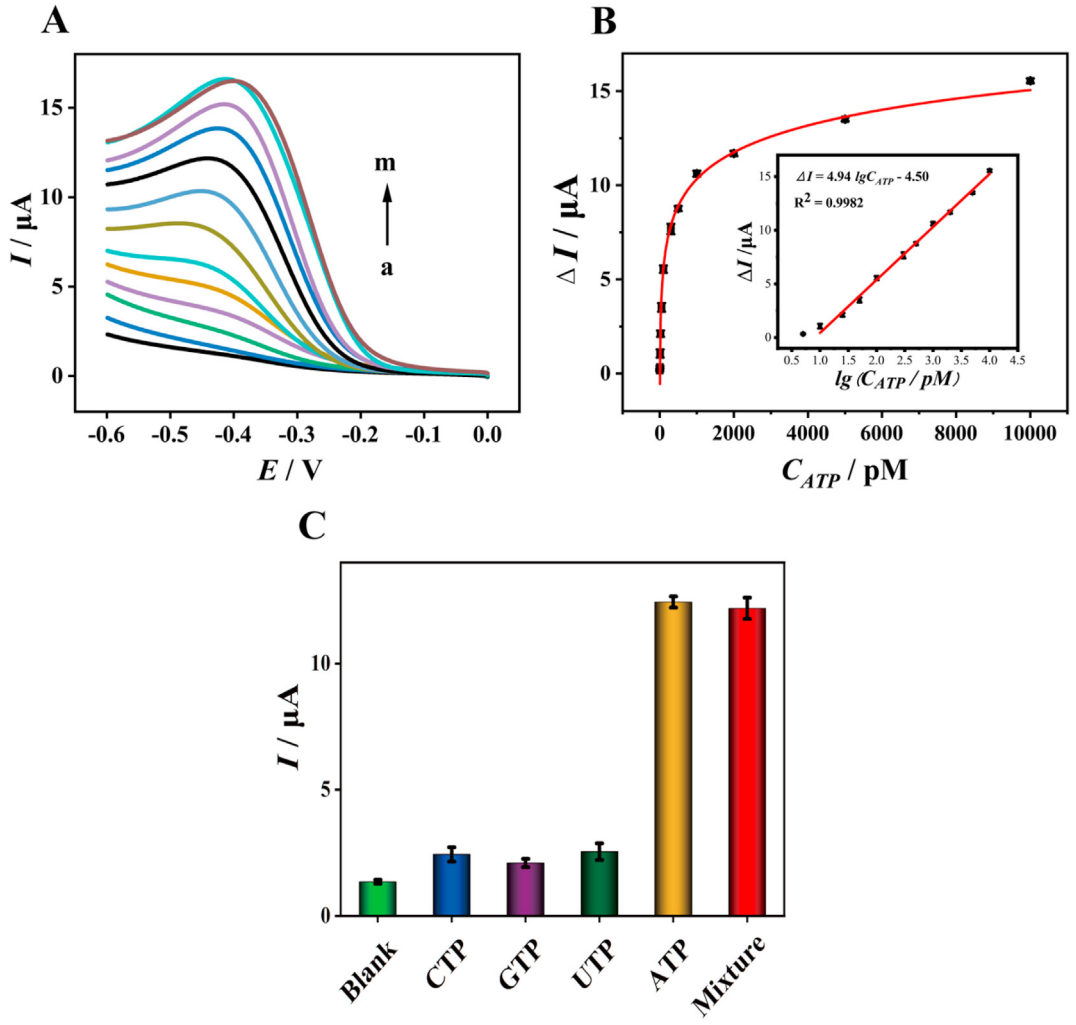

Fig. 4. (A) LSV responses of the modified electrode measured at various ATP concentrations, ranging from a to m as follows: 0, 5, 10, 25, 50, 100, 300, 500, 1000, 2000, 5000, 10000, and 12000 pM, respectively. LSV was performed in PBS containing 1 mM H_2O_2; (B) calibration curve of the ATP sensor. The curve is plotted for the peak LSV current intensity vs ATP concentration. The inset shows the corresponding calibration plot between the peak current and the logarithm of ATP concentration. $\Delta I = I - I_0$, I and I_0 represents the peak current intensity in the presence and absence of ATP in the detection system, respectively; (C) selectivity of the electrochemical biosensors toward the blank control, GTP (50 nM) CTP (50 nM), UTP (50 nM), ATP (5 nM), and a mixture (50 nM of GTP, CTP, and UTP, and 5 nM ATP, respectively). The error bars indicate the standard deviation of five analyses.

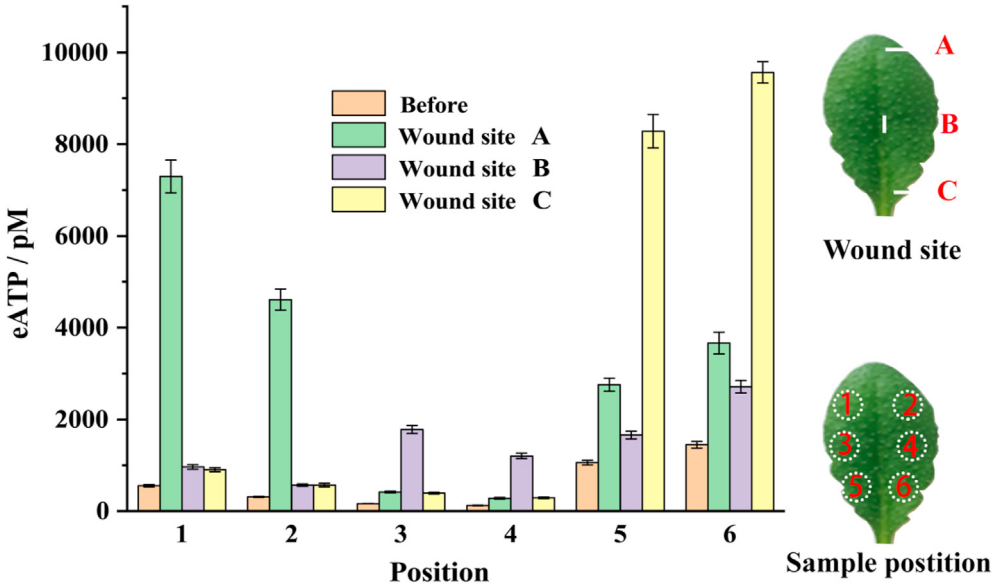

Fig. 5. The level and position effect of extracellular ATP (eATP) before and after infliction of wounds on Arabidopsis leaf. The error bars indicate the standard deviation of five analyses.

detection limit at the 5-pM level was achieved. The utility was also successfully verified in biological samples, suggesting its bioanalytical application potential for the detectection or even mapping of eATP production in plants. Finally, considering the variety of available aptamers, this strategy can be easily extended to analyze different types of biomolecules with the introduction of other nucleic acid amplifications.

CRediT authorship contribution statement

Guoyan Zhao: Conceptualization, Methodology, Investigation, Formal analysis, Writing – original draft. **Yongmei Liu:** Methodology, Investigation, Validation. **Jie Du:** Conceptualization, Writing – review & editing, Supervision, Project administration, Funding acquisition. **Huizi Zhang:** Formal analysis, Resources. **Hanqing Feng:** Visualization, Data curation, Funding acquisition. **Xiaoquan Lu:** Conceptualization, Writing – review & editing, Supervision, Project administration.

Declaration of competing interest

The authors declare that they have no known competing financial interests or personal relationships that could have appeared to influence the work reported in this paper.

Funding and Acknowledgement

This work was supported by National Natural Science Foundation of China (Nos.21565020, 31870246).

Appendix A. Supplementary data

Supplementary data to this article can be found online at https://doi.org/10.1016/j.aca.2021.338681.

References

[1] V. Demidchik, C. Nichols, M. Oliynyk, A. Dark, B.J. Glover, J.M. Davies, Is ATP a signaling agent in plants? Plant Physiol. 133 (2003) 456–461.
[2] S. Chivasa, B.K. Ndimba, W.J. Simon, K. Lindsey, A.R. Slabas, Extracellular ATP functions as an endogenous external metabolite regulating plant cell viability, Plant Cell 17 (2005) 3019–3034.
[3] S. Chivasa, A.M. Murphy, J.M. Hamilton, K. Lindsey, J.P. Carr, A.R. Slabas, Extracellular ATP is a regulator of pathogen defence in plants, Plant J. 60 (2009) 436–448.
[4] M. Pietrowska-Borek, J. Dobrogojski, E. Sobieszczuk-Nowicka, S. Borek, New insight into plant signaling: extracellular ATP and uncommon nucleotides, Cells (2020) 9.
[5] E. Matthus, J. Sun, L.M. Wang, M.G. Bhat, A.B. Mohammad-Sidik, K.A. Wilkins, N. Leblanc-Fournier, V. Legue, B. Moulia, G. Stacey, J.M. Davies, DORN1/P2K1 and purino-calcium signalling in plants: making waves with extracellular ATP, Ann. Bot. 124 (2019) 1227–1242.
[6] D. Basu, E.S. Haswell, Plant mechanosensitive ion channels: an ocean of possibilities, Curr. Opin. Plant Biol. 40 (2017) 43–48.
[7] C.J. Song, I. Steinebrunner, X. Wang, S.C. Stout, S.J. Roux, Extracellular ATP induces the accumulation of superoxide via NADPH oxidases in Arabidopsis, Plant Physiol. 140 (2006) 1222–1232.
[8] J. Choi, K. Tanaka, Y.R. Cao, Y. Qi, J. Qiu, Y. Liang, S.Y. Lee, G. Stacey, Identification of a plant receptor for extracellular ATP, Science 343 (2014) 290–294.
[9] Q.W. Wang, L.Y. Jia, D.L. Shi, R.F. Wang, L.N. Lu, J.J. Xie, K. Sun, H.Q. Feng, X. Li, Effects of extracellular ATP on local and systemic responses of bean (Phaseolus vulgaris L) leaves to wounding, Biosc. Biotech. Biochem. 83 (2019) 417–428.
[10] N.C. van de Merbel, Quantitative determination of endogenous compounds in biological samples using chromatographic techniques, Trac. Trends Anal. Chem. 27 (2008) 924–933.
[11] H. Liu, Y.M. Jiang, Y.B. Luo, W.B. Jiang, A simple and rapid determination of ATP, ADP and AMP concentrations in pericarp tissue of litchi fruit by high performance liquid chromatography, Food Technol. Biotechnol. 44 (2006) 531–534.
[12] T. Qian, Z. Cai, M.S. Yang, Determination of adenosine nucleotides in cultured cells by ion-pairing liquid chromatography–electrospray ionization mass spectrometry, Anal. Biochem. 325 (2004) 77–84.
[13] H. Kim, P. Kosinski, C. Kung, L. Dang, Y. Chen, H. Yang, Y.S. Chen, J. Kramer, G.W. Liu, A fit-for-purpose LC-MS/MS method for the simultaneous quantitation of ATP and 2,3-DPG in human K(2)EDTA whole blood, J. Chromatogr. B-Anal. Technol. Biomed. Life Sci. 1061 (2017) 89–96.
[14] S. Coco, F. Calegari, E. Pravettoni, D. Pozzi, E. Taverna, P. Rosa, M. Matteoli, C. Verderio, Storage and release of ATP from Astrocytes in culture, J. Biol. Chem. 278 (2003) 1354–1362.
[15] P. Turina, D. Samoray, P. Graber, H+/ATP ratio of proton transport-coupled ATP synthesis and hydrolysis catalysed by CF0F1-liposomes, EMBO J. 22 (2003) 418–426.
[16] D. Zheng, D.S. Seferos, D.A. Giljohann, P.C. Patel, C.A. Mirkin, Aptamer nanoflares for molecular detection in living cells, Nano Lett. 9 (2009) 3258–3261.
[17] J. Wang, Y.X. Jiang, C.S. Zhou, X.H. Fang, Aptamer-based ATP assay using a luminescent light switching complex, Anal. Chem. 77 (2005) 3542–3546.
[18] J. Wang, L.H. Wang, X.F. Liu, Z.Q. Liang, S.P. Song, W.X. Li, G.X. Li, C.H. Fan, A gold nanoparticle-based aptamer target binding readout for ATP assay, Adv. Mater. 19 (2007) 3943–3946.
[19] X.L. Zuo, S.P. Song, J. Zhang, D. Pan, L.H. Wang, C.H. Fan, A target-responsive electrochemical aptamer switch (TREAS) for reagentless detection of nanomolar ATP, J. Am. Chem. Soc. 129 (2007) 1042–1043.
[20] N. Arroyo-Curras, P. Dauphin-Ducharme, G. Ortega, K.L. Ploense, T.E. Kippin, K.W. Plaxco, Subsecond-resolved molecular measurements in the living body using chronoamperometrically interrogated aptamer-based sensors, ACS Sens. 3 (2018) 360–366.
[21] Y. Du, B.L. Li, H. Wei, Y.L. Wang, E.K. Wang, Multifunctional label-free electrochemical biosensor based on an integrated aptamer, Anal. Chem. 80 (2008) 5110–5117.
[22] X. Ji, J. Wang, S. Niu, C. Ding, Size-controlled DNA-cross-linked hydrogel coated silica nanoparticles served as a ratiometric fluorescent probe for the detection of adenosine triphosphate in living cells, Chem. Commun. 55 (2019) 5243–5246.
[23] Y.M. Wang, J.W. Liu, L.Y. Duan, S.J. Liu, J.H. Jiang, Aptamer-based fluorometric determination of ATP by using target-cycling strand displacement amplification and copper nanoclusters, Microchim. Acta 184 (2017) 4183–4188.
[24] L. Ge, W.X. Wang, X.M. Sun, T. Hou, F. Li, Affinity-mediated homogeneous electrochemical aptasensor on a graphene platform for ultrasensitive biomolecule detection via exonuclease-assisted target-analog recycling amplification, Anal. Chem. 88 (2016) 2212–2219.
[25] Y. Li, Y. Zeng, X.T. Ji, X. Li, R. Ren, Cascade signal amplification for sensitive detection of cancer cell based on self-assembly of DNA scaffold and rolling circle amplification, Sensor. Actuator. B Chem. 171 (2012) 361–366.
[26] X.J. Ding, W. Cheng, Y.J. Li, J.L. Wu, X.M. Li, Q. Cheng, S.J. Ding, An enzyme-free surface plasmon resonance biosensing strategy for detection of DNA and small molecule based on nonlinear hybridization chain reaction, Biosens. Bioelectron. 87 (2017) 345–351.
[27] Y. Peng, D.X. Li, R. Yuan, Y. Xiang, A catalytic and dual recycling amplification ATP sensor based on target driven allosteric structure switching of aptamer beacons, Biosens. Bioelectron. 105 (2018) 1–5.
[28] S.W. Liu, N.H. Xu, C.Y. Tan, W. Fang, Y. Tan, Y.Y. Jiang, A sensitive colorimetric aptasensor based on trivalent peroxidase-mimic DNAzyme and magnetic nanoparticles, Anal. Chim. Acta 1018 (2018) 86–93.
[29] M.P. Robertson, A.D. Ellington, In vitro selection of an allosteric ribozyme that transduces analytes to amplicons, Nat. Biotechnol. 17 (1999) 62–66.
[30] J.W. Liu, Y. Lu, Adenosine-dependent assembly of aptazyme-functionalized gold nanoparticles and its application as a colorimetric biosensor, Anal. Chem. 76 (2004) 1627–1632.
[31] Y. Yokobayashi, Aptamer-based and aptazyme-based riboswitches in mammalian cells, Curr. Opin. Chem. Biol. 52 (2019) 72–78.
[32] Z.Q. Ning, Y.J. Zheng, D. Pan, Y.J. Zhang, Y.F. Shen, Coupling aptazyme and catalytic hairpin assembly for cascaded dual signal amplified electrochemiluminescence biosensing, Biosens. Bioelectron. 150 (2020) 7.
[33] X. Li, J. Yang, J. Xie, B. Jiang, R. Yuan, Y. Xiang, Cascaded signal amplification via target-triggered formation of aptazyme for sensitive electrochemical detection of ATP, Biosens. Bioelectron. 102 (2018) 296–300.
[34] Y. Chu, A.-P. Deng, W. Wang, J.-J. Zhu, Concatenated catalytic hairpin assembly/hyperbranched hybridization chain reaction based enzyme-free signal amplification for the sensitive photoelectrochemical detection of human telomerase RNA, Anal. Chem. 91 (2019) 3619–3627.
[35] D. Sun, J. Lu, Z. Luo, L. Zhang, P. Liu, Z. Chen, Competitive electrochemical platform for ultrasensitive cytosensing of liver cancer cells by using nanotetrahedra structure with rolling circle amplification, Biosens. Bioelectron. 120 (2018) 8–14.
[36] Z. Chen, Y. Liu, C. Xin, J. Zhao, S. Liu, A cascade autocatalytic strand displacement amplification and hybridization chain reaction event for label-free and ultrasensitive electrochemical nucleic acid biosensing, Biosens. Bioelectron. 113 (2018) 1–8.
[37] H. Pei, L. Liang, G. Yao, J. Li, Q. Huang, C. Fan, Reconfigurable three-dimensional DNA nanostructures for the construction of intracellular logic sensors, Angew. Chem. Int. Ed. 51 (2012) 9020–9024.
[38] D. Chen, D. Sun, Z. Wang, W. Qin, L. Chen, L. Zhou, Y. Zhang, A DNA nanostructured aptasensor for the sensitive electrochemical detection of HepG2 cells based on multibranched hybridization chain reaction amplification strategy, Biosens. Bioelectron. 117 (2018) 416–421.
[39] J. Wang, D.X. Wang, J.Y. Ma, Y.X. Wang, D.M. Kong, Three-dimensional DNA nanostructures to improve the hyperbranched hybridization chain reaction, Chem. Sci. 10 (2019) 9758–9767.

[40] H. Pei, N. Lu, Y. Wen, S. Song, Y. Liu, H. Yan, C. Fan, A DNA nanostructure-based biomolecular probe carrier platform for electrochemical biosensing, Adv. Mater. 22 (2010) 4754–4758.
[41] Y. Wen, H. Pei, Y. Shen, J. Xi, M. Lin, N. Lu, X. Shen, J. Li, C. Fan, DNA Nanostructure-based Interfacial engineering for PCR-free ultrasensitive electrochemical analysis of microRNA, Sci. Rep. 2 (2012) 867.
[42] Z. Ge, M. Lin, P. Wang, H. Pei, J. Yan, J. Shi, Q. Huang, D. He, C. Fan, X. Zuo, Hybridization chain reaction amplification of MicroRNA detection with a tetrahedral DNA nanostructure-based electrochemical biosensor, Anal. Chem. 86 (2014) 2124–2130.
[43] S. Wang, L. Zhang, S. Wan, S. Cansiz, C. Cui, Y. Liu, R. Cai, C. Hong, I.T. Teng, M. Shi, Y. Wu, Y. Dong, W. Tan, Aptasensor with expanded nucleotide using DNA nanotetrahedra for electrochemical detection of cancerous exosomes, ACS Nano 11 (2017) 3943–3949.
[44] L. Zhu, J. Ye, S. Wang, M. Yan, Q. Zhu, J. Huang, X. Yang, Dual amplification ratiometric biosensor based on a DNA tetrahedron nanostructure and hybridization chain reaction for the ultrasensitive detection of microRNA-133a, Chem. Commun. 55 (2019) 11551–11554.
[45] N.-N. Bu, A. Gao, X.-W. He, X.-B. Yin, Electrochemiluminescent biosensor of ATP using tetrahedron structured DNA and a functional oligonucleotide for Ru(phen)32+ intercalation and target identification, Biosens. Bioelectron. 43 (2013) 200–204.
[46] Y. Sun, Q. Wang, L. Mi, L. Shi, T. Li, Target-induced payload amplification for spherical nucleic acid enzyme (SNAzyme)-Catalyzed electrochemiluminescence detection of circulating microRNAs, Anal. Chem. 91 (2019) 12948–12953.
[47] Y. Sun, L. Shi, Q. Wang, L. Mi, T. Li, Spherical nucleic acid enzyme (SNAzyme) boosted chemiluminescence miRNA imaging using a smartphone, Anal. Chem. 91 (2019) 3652–3658.
[48] M. Lin, P. Song, G. Zhou, X. Zuo, A. Aldalbahi, X. Lou, J. Shi, C. Fan, Electrochemical detection of nucleic acids, proteins, small molecules and cells using a DNA-nanostructure-based universal biosensing platform, Nat. Protoc. 11 (2016) 1244.
[49] Q.Z. Hou, Y.P. Wang, B.Q. Fan, K. Sun, J.Y. Liang, H.Q. Feng, L.Y. Jia, Extracellular ATP affects cell viability, respiratory O-2 uptake, and intracellular ATP production of tobacco cell suspension culture in response to hydrogen peroxide-induced oxidative stress, Biologia, 7.
[50] L.Y. Jia, J.Y. Bai, K. Sun, R.F. Wang, H.Q. Feng, Extracellular ATP released by copper stress could act as diffusible signal in alleviating the copper stress-induced cell death, Protoplasma 256 (2019) 491–501.
[51] J. Li, W. Zheng, A.H. Kwon, Y. Lu, In vitro selection and characterization of a highly efficient Zn(II)-dependent RNA-cleaving deoxyribozyme, Nucleic Acids Res. 28 (2000) 481–488.
[52] D.E. Huizenga, J.W. Szostak, A DNA aptamer that binds adenosine and ATP, Biochemistry 34 (1995) 656–665.
[53] L. Liu, J. Du, W.-e. Liu, Y. Guo, G. Wu, W. Qi, X. Lu, Enhanced His@AuNCs oxidase-like activity by reduced graphene oxide and its application for colorimetric and electrochemical detection of nitrite, Anal. Bioanal. Chem. 411 (2019) 2189–2200.
[54] Y. Wan, H. Xu, Y. Su, X. Zhu, S. Song, C. Fan, A surface-initiated enzymatic polymerization strategy for electrochemical DNA sensors, Biosens. Bioelectron. 41 (2013) 526–531.
[55] S. Liu, C. Wang, C. Zhang, Y. Wang, B. Tang, Label-free and ultrasensitive electrochemical detection of nucleic acids based on autocatalytic and exonuclease III-assisted target recycling strategy, Anal. Chem. 85 (2013) 2282–2288.
[56] Y. Lv, S. Chen, Y. Shen, J. Ji, Q. Zhou, S. Liu, Y. Zhang, Competitive multiple-mechanism-driven electrochemiluminescent detection of 8-Hydroxy-2′-deoxyguanosine, J. Am. Chem. Soc. 140 (2018) 2801–2804.
[57] J. Tang, L. Hou, D. Tang, B. Zhang, J. Zhou, G. Chen, Hemin/G-quadruplex-based DNAzyme concatamers as electrocatalysts and biolabels for amplified electrochemical immunosensing of IgG1, Chem. Commun. 48 (2012) 8180–8182.
[58] M. Lin, J. Wang, G. Zhou, J. Wang, N. Wu, J. Lu, J. Gao, X. Chen, J. Shi, X. Zuo, C. Fan, Programmable engineering of a biosensing interface with tetrahedral DNA nanostructures for ultrasensitive DNA detection, Angew. Chem. Int. Ed. 54 (2015) 2151–2155.
[59] D.C. Vanegas, G. Clark, A.E. Cannon, S. Roux, P. Chaturvedi, E.S. McLamore, A self-referencing biosensor for real-time monitoring of physiological ATP transport in plant systems, Biosens. Bioelectron. 74 (2015) 37–44.
[60] S.Y. Kim, M. Sivaguru, G. Stacey, Extracellular ATP in plants. Visualization, localization, and analysis of physiological significance in growth and signaling, Plant Physiol. 142 (2006) 984–992.